# Terpolymers from Lactide and Bisphenol A Derivatives: Scale-Up, Properties, and Blends

**Akhilesh Singh,[1*] Amit K. Naskar,[2†] Joel Barden,[2] Michael J. Drews,[1] Dennis W. Smith, Jr.[1,2,3‡]**

[1]*School of Material Science and Engineering, Clemson University, Clemson, South Carolina 29634*
[2]*Department of Chemistry, Clemson University, Clemson, South Carolina 29634*
[3]*Center for Optical Materials Science and Engineering Technologies (COMSET) and Advanced Materials Research Laboratory, Clemson University, Clemson, South Carolina 29634*

Received 22 May 2010; accepted 22 November 2010
DOI 10.1002/app.33789
Published online 23 June 2011 in Wiley Online Library (wileyonlinelibrary.com).

**ABSTRACT:** Terpolymerization of L-lactide (LA) and bisphenol A derivatives was performed on few hundred gram scale, and the resultant terpolymer (TP) was characterized by gel permeation chromatography, infrared spectroscopy (FTIR), differential scanning calorimetry (DSC), dynamic mechanical analysis (DMA), and thermogravimetric analysis. Moderate molecular weight ($M_n \sim 12$ kg/mol) TP was achieved with glass transition temperatures about 100°C (DSC and DMA). The TP exhibited improved thermal stability compared with polylactide (PLA), with a thermal degradation temperature of about 80°C higher than PLA. Although the TP exhibited distinctly different surface morphology compared with that of PLA, both showed similar contact angle and surface energy (ca. 40 mN/m) properties. Blends of PLA and TP showed enhanced glass transition ($\sim$ 5°C change in $T_g$) temperatures compared with PLA homopolymer. This is due to the compatibility of PLA and TP. Thus, TP could be used as an additive for PLA-based blends to enhance compatibility with phenolic-based resins. TP electrospun fiber morphology is also reported. © 2011 Wiley Periodicals, Inc. J Appl Polym Sci 122: 2520–2528, 2011

**Key words:** glass transition; ring-opening polymerization; thermal properties; blends; structure–property relations

## INTRODUCTION

The chemical industry worldwide uses about 12% of fossil feedstocks for energy generation and as raw materials. These fossil feedstocks account for more than 90% of the raw materials in the chemical industry, and a large portion of these are used for producing polymers.[1] High-performance polymers produced from renewable resources are expected to become an attractive alternative to petroleum feedstock-based materials in the future and may help to alleviate cost, sustainability, and environmental concerns.

One such renewable resource-derived polymer is polylactide or poly(lactic acid) (PLA). The first synthesis of PLA was reported by Carothers et al in 1932.[2] The medical applications of PLA and its copolymers, for surgical implants and tissue repair, began in the 1960s.[3] In addition to the biomedical and pharmaceutical applications, PLA and its copolymers are showing a rise in their use in commodity applications because of mechanical properties approaching those of some petroleum-based polymers, their compostability with low toxicity, and indications of reduced price.[4] The widespread use of PLA is currently limited because of its unfortunate glass transition temperature range (50–60°C) compared with competing plastics such as polystyrene (ca. 100°C).[5,6]

Various modification routes for PLA have been used to alter the intrinsic properties. Enhancement of properties by the use of novel catalysts and modifications by blending, plasticization, and copolymerization with other polymers and/or compounds have recently been reported.[5,7–9] Earlier, we reported a terpolymer (TP) based on lactide (LA) and bisphenol A derivatives, which exhibited glass transition temperatures about 80°C.[6] Here, a scaled-up synthesis of polymer produced from LA, 4,4′-hexafluoroisopropylidenediphenol (6F-Bis-A), and the diglycidyl ether of bisphenol A (DGEBA), its characterization, and utilization in PLA blends are reported.

**Present address:* Tetramer Technologies, L.L.C., 657 S. Mechanic Street, Pendleton, SC 29670.
†*Present address:* Materials Science and Technology Division, Oak Ridge National Laboratory, Oak Ridge, TN 37831-6053.
‡*Present address:* Department of Chemistry, The University of Texas at Dallas, 800 W Campbell Rd. BE26, Richardson, TX 7580-3021..
*Correspondence to:* D. W. Smith, Jr. (dwsmith@utdallas.edu).
Contract grant sponsors: DARPA, National Textiles Center (US Department of Commerce).

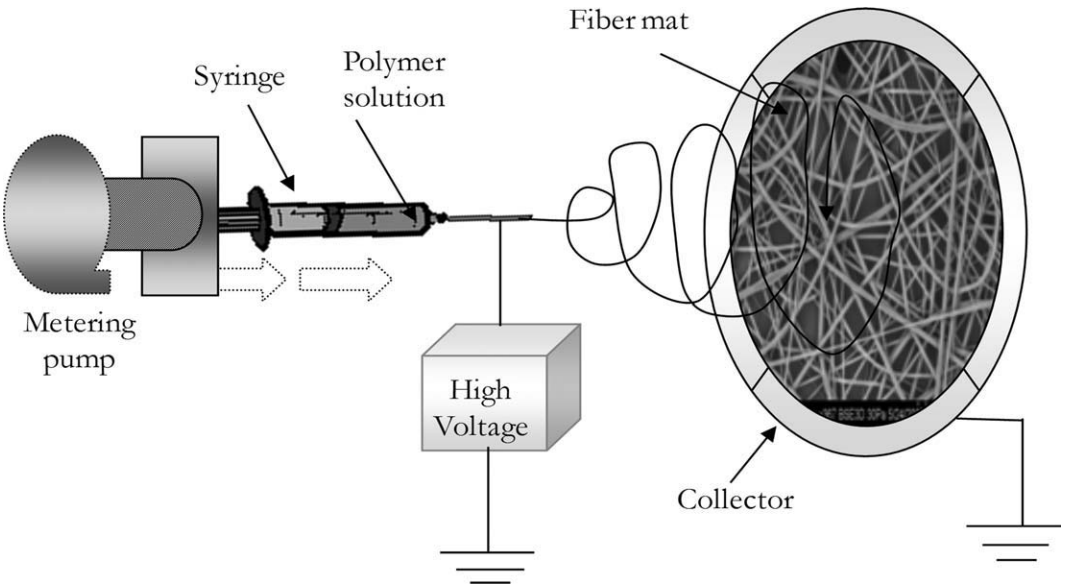


**Figure 1** Schematic of electrospinning process for fiber spinning.

## MATERIALS AND METHODS

L-Lactide was generously donated by Poly-Med (Pendleton, SC) and was recrystallized from ethyl acetate and vacuum dried before use. Polylactide (Polymer 4042D) was generously donated by Cargill Dow Polymers, LLC (now NatureWorks LLC). Diglycidyl ether of bisphenol A, 4,4′-(hexafluoroisopropylidene)diphenol, and 1-phenoxy-2-propanol (Dowanol$^{TM}$) were generously donated by The Dow Chemical Company (Freeport, TX) and were used as received. Potassium chloride (KCl) and 18-Crown-6 (18C6) were purchased from Sigma Aldrich (USA) and were used as received. All other chemicals and reagents were purchased from Fisher or Sigma Aldrich and were used as received unless otherwise stated.

### Scaled-up synthesis of terpolymer

The terpolymerization of LA, DGEBA, and 6F-Bis-A was carried out using equimolar ratios of the three components. A typical reaction mixture was prepared by adding 1 equiv each of LA, DGEBA, and 6F-Bis-A; 2.7 mequiv of KCl, 2.9 mequiv of 18C6E, and 0.7 equiv of Dowanol$^{TM}$. The catalyst system (KCl and 18C6) was stirred overnight in about 10 mL Dowanol$^{TM}$ before use. The reaction mixture ($\sim$ 300 g) was added to a 1-L stainless steel Parr

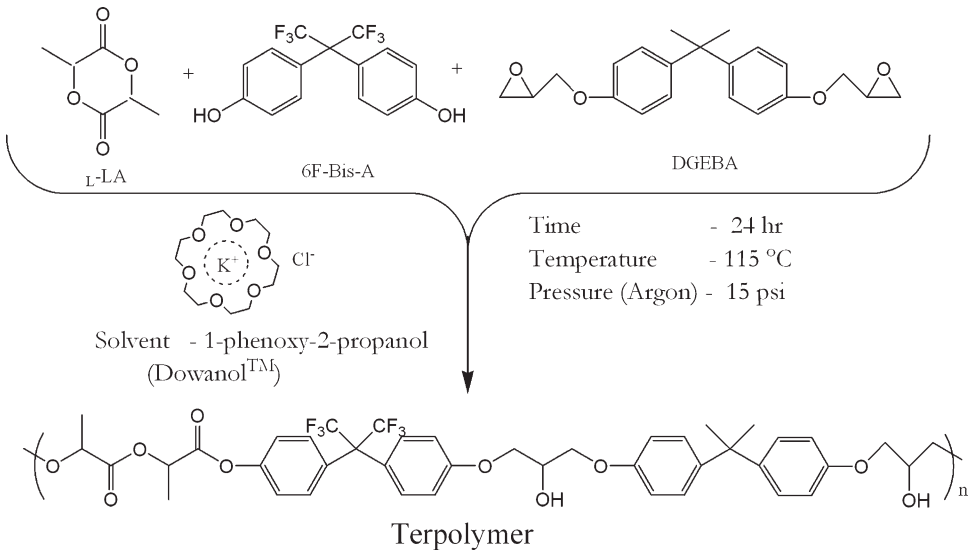


**Scheme 1** Terpolymerization of L-lactide and bisphenol A derivatives (DGEBA and 6F-Bis-A).

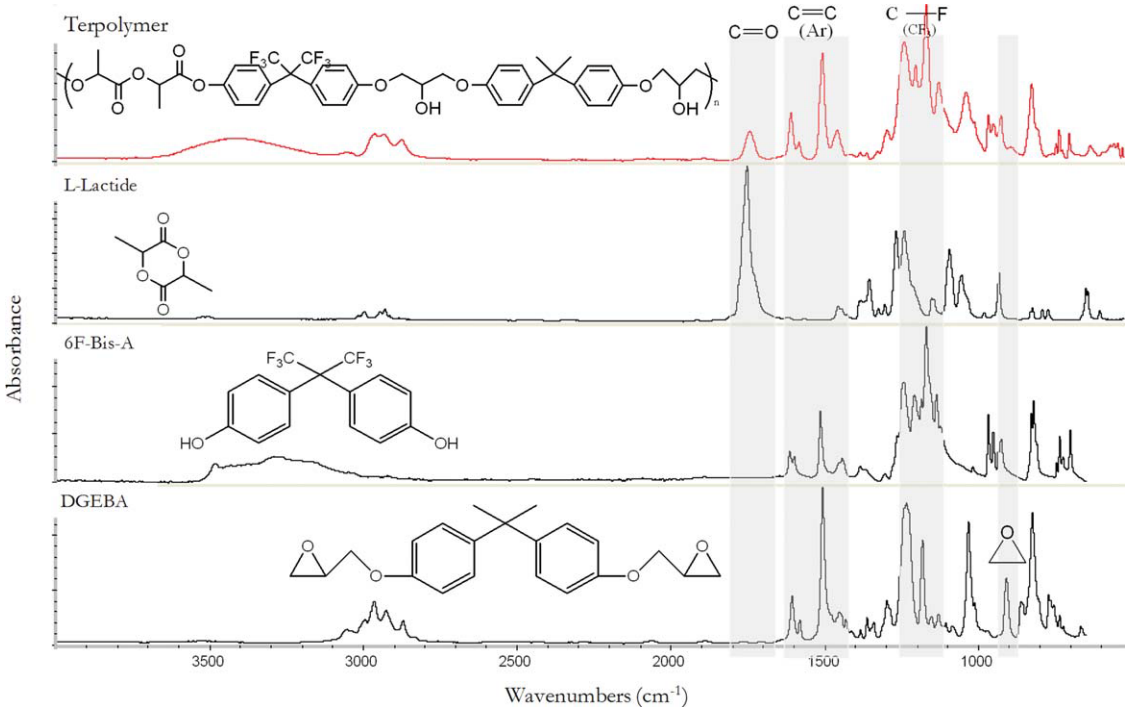


**Figure 2** FTIR spectra for TP, L-lactide, 6F-Bis-A, and DGEBA. [Color figure can be viewed in the online issue, which is available at wileyonlinelibrary.com.]

reactor, purged, and sealed under 15 psi of argon at room temperature. The temperature was gradually (~ 2°C/min) increased to 115°C and held for 24 h with stirring (20 rpm) throughout. The terpolymerization product was removed via bottom drain valve and cooled. The reaction product was dissolved in tetrahydrofuran (THF) and precipitated by addition to methanol and then redissolved in THF and precipitated by addition to *n*-hexane. The precipitated TP was then vacuum dried at 90°C for 1 h. Typical TP yields after precipitation ranged from 80 to 90%.

## Characterization

FTIR spectroscopy was performed using a Thermo-Nicolet Magna-IR™ 550 spectrometer (Thermo Nicolet, Waltham, MA) equipped with a Thermo Spectra-Tech Foundation Series Endurance diamond attenuated total reflectance accessory. Data were analyzed using OMNIC E.S.P. v 7.2 software.

Differential scanning calorimetry (DSC) analysis was conducted using a TA Instruments (New Castle, DE) Q1000 DSC. Data were analyzed using TA Instruments Universal Analysis 2000 version 4.1D software. The samples (6–8 mg in standard aluminum pans) were initially heated to 225°C to erase the prior thermal history, then cooled to −50°C, and finally heated from −50 to 225°C. A heating rate of

**TABLE I**
**The FTIR Peak Assignment for Lactide, 6F-Bis-A, DGEB, and TP**

| | FTIR peaks assignment, wavenumber ($cm^{-1}$) | | | |
|---|---|---|---|---|
| Functional group | Lactide | 6F-Bis-A | DGEBA | TP |
| C=O | 1753 | – | – | 1743 |
| Epoxy stretch | – | – | 911 | – |
| C=C (aromatic) | – | 1615/1515 | 1607/1508 | 1608/1510 |
| C—F from —$CF_3$ | – | 1170 | – | 1170 |
| Ph—O—C | – | – | 1298 | 1297 |

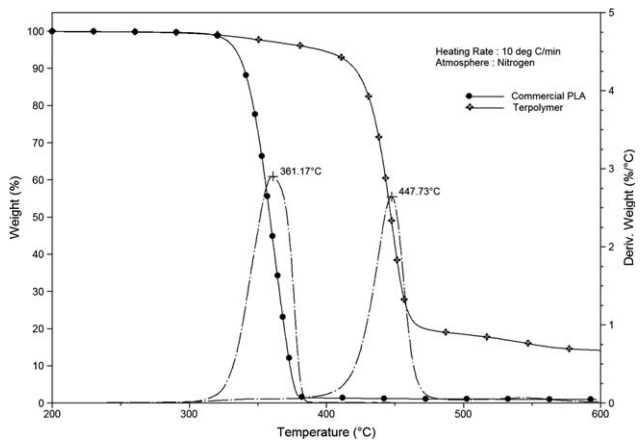


**Figure 3** Thermogravimetric analysis of PLA and TP demonstrating the percentage weight loss and rate of weight loss as a function of temperature (under nitrogen). Broken lines represent the derivative weight loss plots of corresponding TGA profiles.

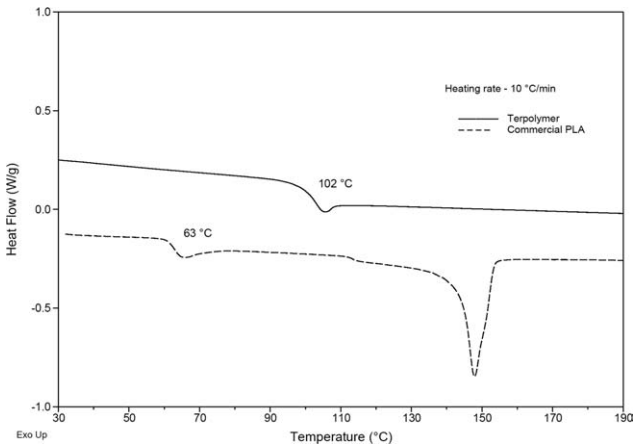


**Figure 4** DSC thermograms comparing the observed thermal transitions for PLA and TP.

10°C was used for all of the segments described above. Glass transition temperatures were measured based on the inflection point of the step transition. Temperature values of the endothermic and exothermic peak maxima are reported as the melting and crystallization temperatures, and the peak area was used to calculate heats of fusion and crystallization, respectively.

Thermal gravimetric analysis (TGA) was conducted using a TA Instruments (New Castle, DE) 2950 TGA. Data were analyzed using TA Instruments Universal Analysis 2000 version 4.1D software. Samples were heated at a rate of 10°C/min from room temperature to 400°C under a nitrogen purge.

Dynamic mechanical analysis was performed using a DMS 210 Tension Module (Seiko Instruments, Japan) with specimen dimensions of 40 mm × 10 mm and an effective gauge length of 20 mm. Samples were evaluated over a temperature range of −130 to

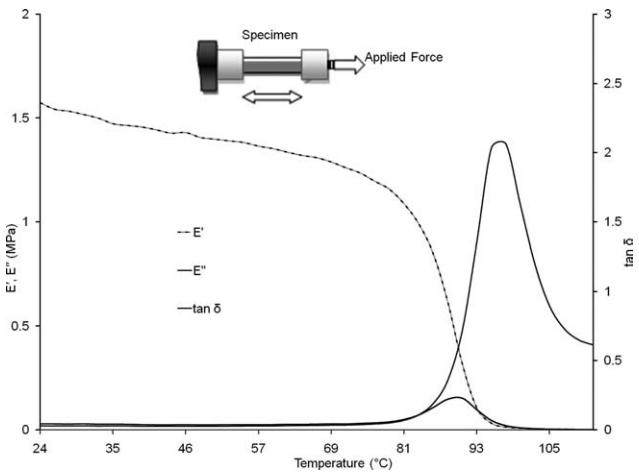


**Figure 5** Dynamic mechanical analysis curve with storage modulus ($E'$), loss modulus ($E''$), and loss factor (tan δ) for TP.

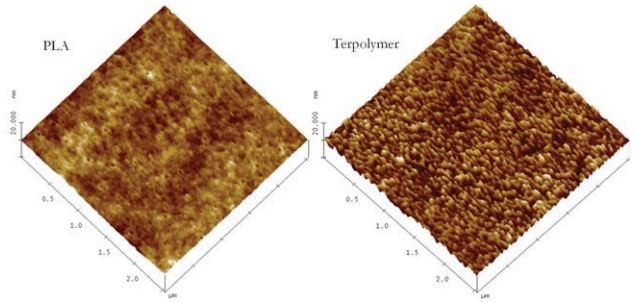


**Figure 6** AFM topography images of PLA (left) and TP (right) with a scan size of 2.5 μm × 2.5 μm. [Color figure can be viewed in the online issue, which is available at wileyonlinelibrary.com.]

125°C at a heating rate of 2°C/min at a frequency of 1 Hz and a deformation amplitude of 10 μm. Data were analyzed using EXSTAR6000 software.

Silicon wafer substrates for atomic force microscope (AFM) studies were oxidized by immersion in piranha solution (three parts 95–98% $H_2SO_4$ + one part 30% $H_2O_2$) at 80°C for 45 min. The thickness of the resultant $SiO_2$ layer was measured by ellipsometry and found to be about 1.4 nm. Solutions of 2% (w/v) homopolymer and TP in chloroform were prepared and filtered through a Whatman 0.2-μm polytetrafluoroethylene membrane syringe filter. Dip coating of oxidized silicon wafers was carried out using a dip coater (Mayer Feintechnik D-3400, Göttingen, Germany). Dip-coated samples were air dried, and the film thicknesses were measured using ellipsometry.

A Dimension 3100 (Veeco, Woodbury, NY) AFM equipped with Nanoscope IIIa controller was used to image the surface of the dip-coated polymer film on silicon wafers. All AFM characterization experiments were performed using a silicon AFM tip (MicroMash, nominal force constant 40 N/m, tip radius < 10 nm) in noncontact (tapping) mode.

Static contact angle measurements were performed using the sessile drop method on a Drop Shape Analysis (KRÜSS Instruments, Hamburg, Germany) system. Liquid drops with an average volume between 5 and 10 μL were placed on the dip-coated polymer

**TABLE II**
**Dispersive and Polar Components of Probe Liquid Surface Energy at 20°C[17]**

| Liquid | Surface energy of liquids (mN/m) | | |
|---|---|---|---|
| | Dispersive component | Polar component | Total surface energy |
| Water | 21.8 | 51.0 | 72.8 |
| Glycerol | 37.0 | 26.4 | 63.4 |
| Formamide | 39.5 | 18.7 | 58.2 |
| Methylene iodide | 48.5 | 2.3 | 50.8 |
| *n*-Hexadecane | 27.6 | 0.0 | 27.6 |

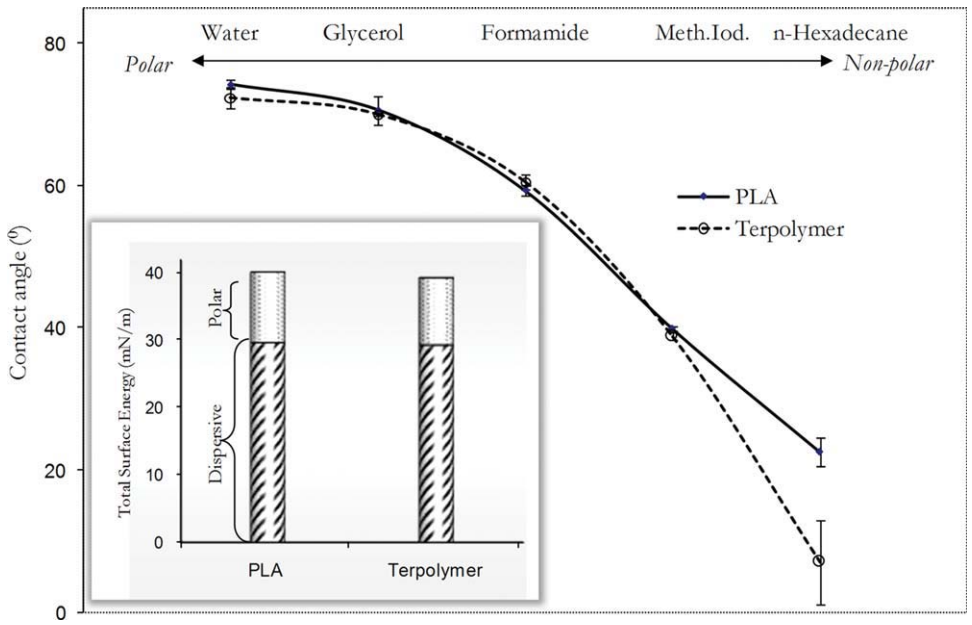


**Figure 7** Static contact angle of water, glycerol, formamide, methylene iodide, and *n*-hexadecane on PLA and TP dip coated on silicon wafers. Inset: Total surface energy and its components for PLA and TP by the Kaelble method.

films, and the equilibrium contact angles were measured after an equilibration time of 30 s.

### Blend preparation

Films were cast from a 2% (w/v) solution of polymer in chloroform. Two grams of PLA, TP, poly(methyl methacrylate) (PMMA), or blend compositions: PLA/TP: 95/5, 85/15, and 55/45 and PLA/PMMA: 85/15 and 55/45 were dissolved in 100 mL chloroform and stirred to obtain a clear solution. Solutions were cast in Teflon dishes and covered with a small vent for slow drying. After 24 h, the films were removed and dried under vacuum at 60°C for 16 h (overnight).

### Electrospinning

Polymer solutions of concentrations between 25 and 35% (w/v) in chloroform and THF were electrospun using the electrospinning equipment illustrated in Figure 1. Solutions were placed in a 10-mL syringe and then extruded through a 16 ½ gauge needle at a rate of 6 mL/h. A total of 15 kV was applied to the needle, and the polymer jet was collected on a grounded aluminum surface at a distance of 10 cm. The electrospun mat was then vacuum dried at 60°C for 1 h.

Scanning electron microscopy (SEM) images of electrospun fiber samples were obtained using a Hitachi S3400N (Hitachi High-Technologies, Japan) microscope at an accelerating voltage of 20 kV. A Hummer® 6.2 (Anatech, Hayward, CA) sputter coater was used to precoat the samples with a 4- to 5-nm layer of platinum.

## RESULTS AND DISCUSSION

The scaled-up (ca. 300-g batch) terpolymerization of LA, 6F-Bis-A, and DGEBA (TP) was carried out as shown in Scheme 1. Catalyst complexes of 18C6/KCl have been used for the polymerization of epoxides and esters.[6,10,11] The effect of feed ratio and solvent on the terpolymerization is discussed in detail by Abayasinghe and Smith.[6] The equimolar terpolymerization of LA, 6F-Bis-A, and DGEBA at 115°C for 24 h resulted in TPs with molecular weight ($M_n$) of about 12,000 and molecular weight distribution ($M_w/M_n$) of about 1.5.

During LA homopolymerization, the carbanions generated by the attack of nucleophiles are stabilized by a tautomeric equilibrium with the enolate form. The propagation of the reaction proceeds by the alkyl-oxygen bond scission of the LA.[12] The detailed mechanistic aspects of LA polymerization are described by Fish and Dupon, and Jedlinski *et al.*[12,13] For the terpolymerization in this study, some mechanistic aspects have already been reported,[14] and these will be further detailed in a later report.

The amount of incorporation of different moieties in the polymer chain of TP was measured using FTIR spectroscopy as shown in Figure 2. The FTIR spectrum of the TP shows the presence of a peak at 1743 $cm^{-1}$, which corresponds to the carbonyl (C=O) in the ring-opened LA unit compared with 1753 $cm^{-1}$ in the unreacted monomer. The peaks

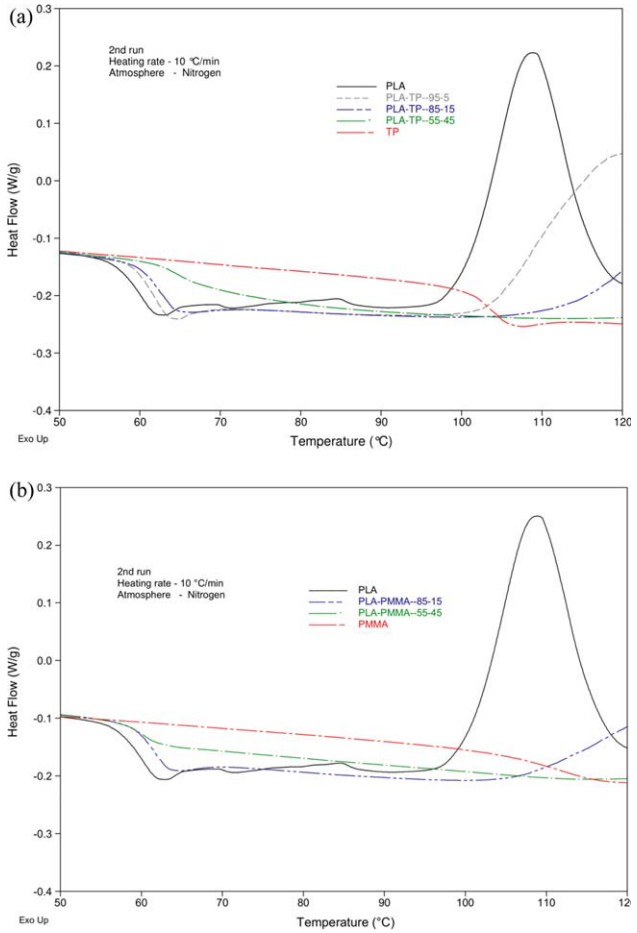


**Figure 8** (a) DSC thermogram of TP/PLA blends. (b) DSC thermogram of PMMA/PLA blends. [Color figure can be viewed in the online issue, which is available at wileyonlinelibrary.com.]

(strong) at about 1610 and 1510 $cm^{-1}$ in 6F-Bis-A, DGEBA, and TP correspond to the aromatic C=C stretch. The C—F stretch from $CF_3$ group in 6F-Bis-A and TP shows a strong peak at 1170 $cm^{-1}$. The epoxy stretching peak at 911 $cm^{-1}$ in DGEBA completely disappears in the TP as expected. The Ph—O—C stretch is observed in the DGEBA and TP at 1297 $cm^{-1}$. The FTIR peak assignments for LA, 6F-Bis-A, DGEB, and TP are summarized in Table I. All other spectroscopic data were consistent with the data reported in our initial communication for the TP shown in Scheme 1 with single LA enchainment.[6]

Structural characteristics, such as structural regularity, bond flexibility, close packing ability, and physical interaction, affect the thermal performance of a polymer.[15,16] Aromatic units are, furthermore, well known to increase thermal resistance and chain rigidity. Weight loss curves (TGA) for PLA and TP are shown in Figure 3. The difference in the maxima of the derivative peaks for PLA and TP is about 86°C, which is remarkable because the TP contains a significant aliphatic polyester component.

The calculated glass transition temperature for the TP using the Bicerano module was about 105°C (Polymer-Design Tools™ version 1.1, DTW Associates). As shown by the comparison of the DSC thermograms in Figure 4, the glass transition temperature of TP is above 100 (102°C), which is about 40°C higher than commercial PLA. No melting peak was observed for the TP.

Figure 5 shows the plot of the storage modulus, loss modulus, and loss factor (tan δ) as a function of temperature for the TP. Analysis was performed on a compression-molded article (40 mm × 10 mm × 1.6mm) of TP. The relatively low storage modulus of <2 MPa at lower temperature range for the TP is due to the moderate molecular weight. The tan δ shows a peak at about 98°C, which is consistent with the DSC data.

## Surface morphology and energy

The AFM surface topography images of PLA and TP are shown in Figure 6. PLA shows a very smooth surface, whereas the TP shows a rough surface morphology. The expected contrast observed is due to the difference in the solubility and viscosity of polymers in chloroform, the crystallinity of PLA, and molecular weight differences.

Static contact angle measurements were performed using the sessile drop method with an equilibration time of 30 s. The probe liquids and corresponding surface energy data[17] are summarized in Table II. Plots of the contact angles of five probe liquids (water, glycerol, formamide, methylene iodide, and *n*-hexadecane) on PLA (synthesized by ring-opening polymerization) and TP are shown in Figure 7. Water has a relatively high surface tension (72 mN/m), and interfacial forces have a significant contribution from intermolecular forces such as hydrogen bonding. In the case of *n*-hexadecane, which has a surface tension of 27 mN/m, only dispersion forces contribute to the

**TABLE III**
**DSC Data for the Different TP Blend Formulations**

| Homopolymer and blends (% composition) | | | First-order and second-order transitions (°C) | | |
|---|---|---|---|---|---|
| PLA | TP | PMMA | $T_g$ | $T_c$ | $T_m$ |
| 100 | – | – | 60 | 109 | 175 |
| 95 | 5 | – | 61 | 122 | 173 |
| 85 | 15 | – | 62 | 134 | 173 |
| 55 | 45 | – | 65 | 143 | 174 |
| – | 100 | – | 104 | – | – |
| 85 | – | 15 | 61 | 132 | 174 |
| 55 | – | 45 | 60 | 143 | 174 |
| – | – | 100 | 112 | – | – |

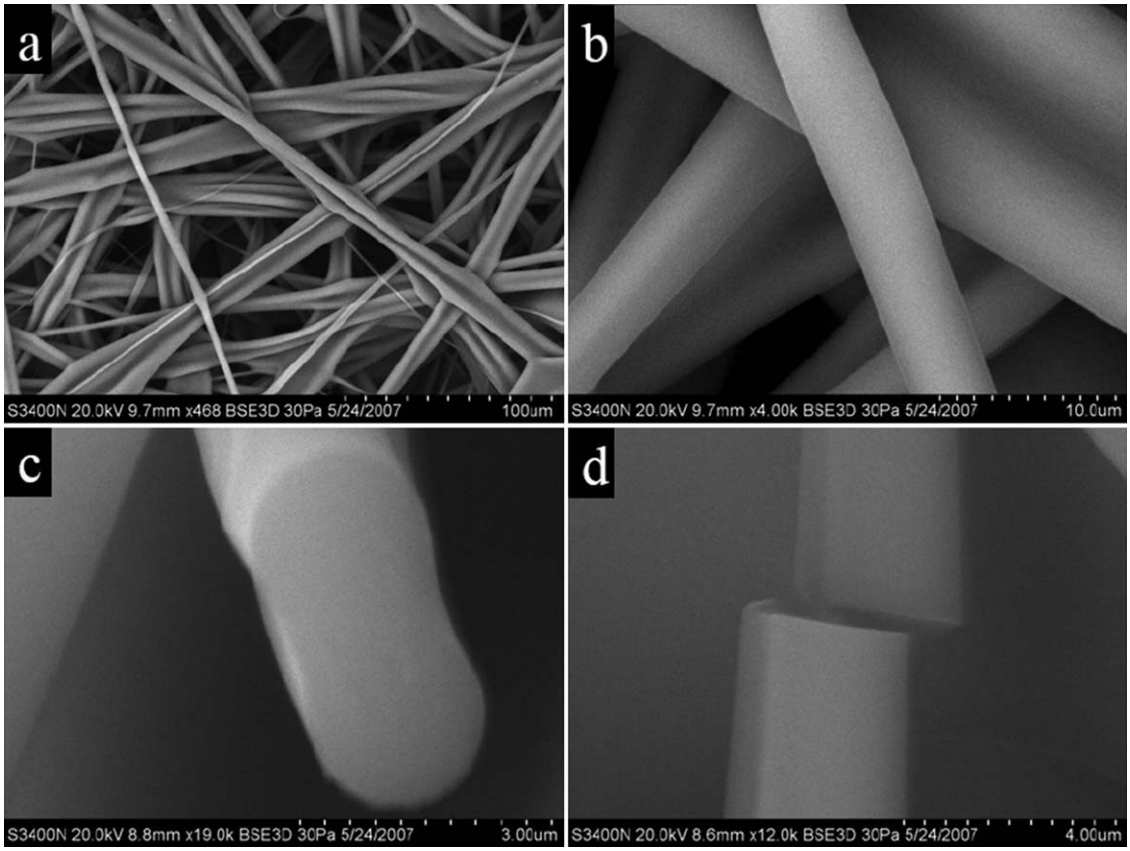


**Figure 9** SEM images of TP fibers electrospun from $CHCl_3$. Images (a) and (b) are at different magnification, and images (c) and (d) show the cross section of fiber after freeze fracture.

interfacial tension. No significant difference in the contact angles of PLA and TP was noted with the test liquids with the exception that TP showed a slightly lower contact angle with *n*-hexadecane.

The Owens–Wendt–Rabel–Kaelble (OWRK) method was used to investigate the surface energies of PLA and TP. The dispersive and polar components of the total surface energies of PLA and TP were obtained by OWRK equation 1:[18]

$$\frac{(1+\mathrm{Cos}\,\theta)}{2}\cdot\frac{\gamma_l}{\sqrt{\gamma_l^{\mathrm{d}}}}=\sqrt{\gamma_s^{\mathrm{d}}}+\sqrt{\gamma_s^{\mathrm{p}}}\cdot\left(\frac{\sqrt{\gamma_l^{\mathrm{p}}}}{\sqrt{\gamma_l^{\mathrm{d}}}}\right), \quad (1)$$

where $\gamma_l, \gamma_l^{\mathrm{d}}, \gamma_l^{\mathrm{p}}$ $\gamma_s^{\mathrm{d}}, \gamma_s^{\mathrm{p}}$ and $\theta$ are the total surface energy of liquid, dispersive component of surface energy for liquid, polar component of surface energy for liquid, dispersive component of surface energy for solid, polar component of surface energy for solid, and contact angle in degrees, respectively. The plots of $\frac{(1+\mathrm{Cos}\theta)}{2}\cdot\frac{\gamma_l}{\sqrt{\gamma_l^{\mathrm{d}}}}$ versus $\frac{\sqrt{\gamma_l^{\mathrm{p}}}}{\sqrt{\gamma_l^{\mathrm{d}}}}$ give values of dispersive and polar components of surface energies of solids. The inset in Figure 7 shows the polar and dispersive component of surface energies of PLA and TP. The dispersive component of surface energy for PLA and TP was 29.7 and 29.4 mN/m, respectively, and the polar component of surface energy for PLA and TP was 10.5 and 10.0 mN/m, respectively. Although the total surface energy of PLA and TP is similar, the effect of surface roughness cannot be ignored. The TP surface has higher roughness (RMS roughness = 0.80 ± 0.10 nm) in comparison to that of PLA (RMS roughness = 0.22 ± 0.02 nm). As the higher roughness can make surface appear more hydrophilic, it is expected that the TP is not be as hydrophilic the data suggest. Studying the effect of surface roughness on the contact angles of these polymers was beyond the scope of this manuscript.

### Thermal analysis of terpolymer blends

The DSC thermograms for TP/PLA and PMMA/PLA blends in different compositions are displayed in Figure 8(a,b). The $T_g$, crystallization temperatures ($T_c$), and melting temperatures ($T_m$) of the films are summarized in Table III. PMMA was selected for blend comparison because of its similar amorphous nature and glass transition temperature of about 100°C. Incorporation of TP or PMMA into PLA does

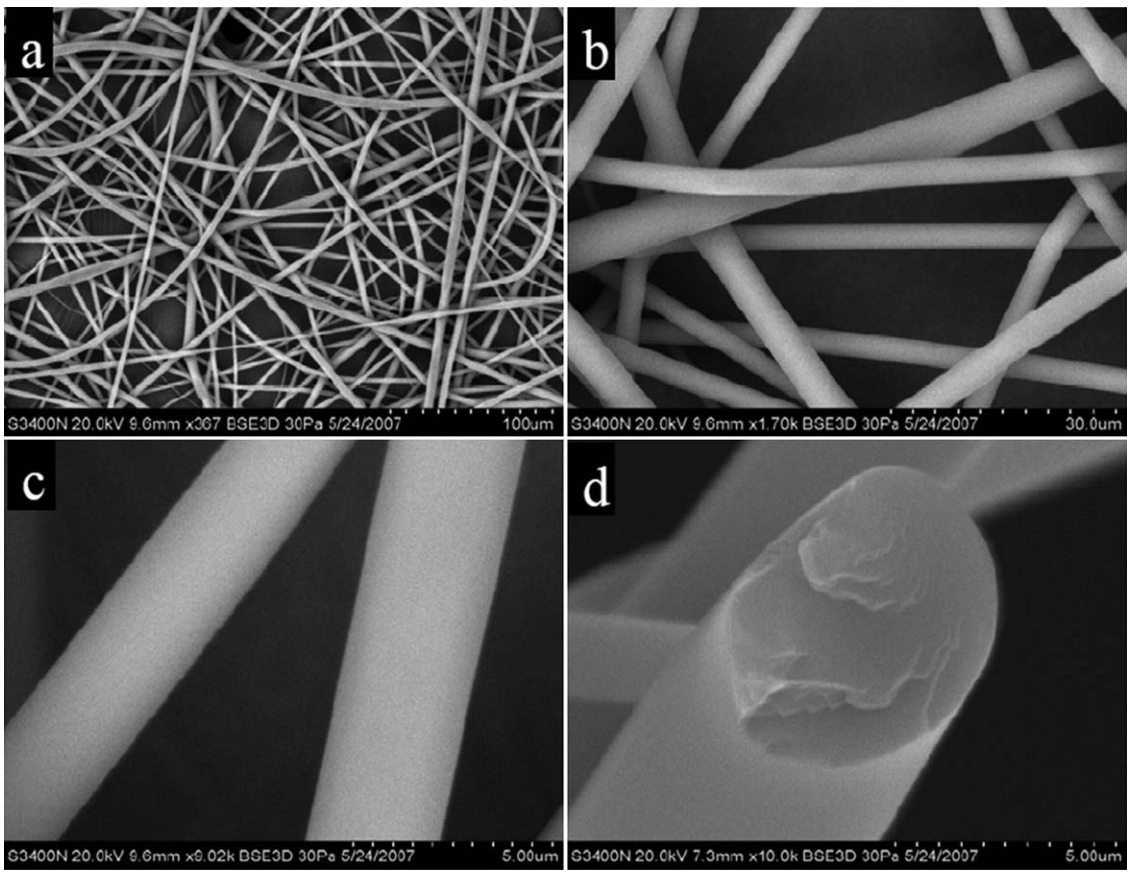


**Figure 10** SEM images of TP fibers electrospun from THF. Images (a), (b), and (c) are at different magnification, and image (d) shows the cross section of fiber after freeze fracture.

not significantly affect the melting temperature of the PLA phase (173–175°C). However, addition of the TP increases the crystallization temperature of PLA significantly. For example, compositions of PLA/TP 100/0, 95/05, and 85/15 exhibit $T_c$ of 109, 122, and 134°C, respectively. As displayed in Figure 8(a), the incorporation of TP shifts the glass transition temperature of the PLA phase to higher temperature. However, although PMMA has higher $T_g$ than TP (112 and 102°C, respectively), blends of PMMA and PLA do not show an increase in $T_g$ of the PLA phase. For example, a 55/45 PLA/TP blend exhibits $T_g$ at 65°C (i.e., 5°C $T_g$ enhancement of PLA matrix); however, a 55/45 PLA/PMMA blend exhibits $T_g$ at 60°C (i.e., no $T_g$ enhancement of the PLA matrix). This data suggest that the TP could be used as a novel compatibilizer for various PLA-based blends.

## Electrospinning

Electrospinning is a versatile, flexible, and convenient technique compared with other micro/nanostructure fabricating methods such as phase separation and template synthesis.[19] A schematic of the electrospinning process and apparatus is shown in Figure 1. Figure 9 exhibits the SEM images of fibers electrospun from a 25% (w/v) of TP in chloroform. Images (a) and (b) show ribbon-like fibers with a few cylindrically shaped fibers. The shape of fiber is strongly dependent on the concentration and thus viscosity of the polymer solution.[20] Concentrations lower than 20% (w/v) resulted in bead formation and short fibers. The low molecular weight of the TP required higher feed concentration to achieve a suitable viscosity for electrospinning. Images (c) and (d) exhibit cross-sectional views of electrospun fibers that were freeze fractured in liquid nitrogen. Image (c) shows the ribbon-like structure, and image (d) shows the nearly cylindrical shape. The brittle fracture can be seen from the cross section of image (c) and (d) as the cross section is very smooth.

Figure 10 shows the SEM images of electrospun fibers from 35% (w/v) solution of TP in THF. Images (a), (b), and (c) show the SEM of the fiber mat at different magnification levels, and image (d) shows the cross section of an electrospun fiber that was freeze fractured in liquid nitrogen. The fibers spun at 35% (w/v) were all cylindrical in shape with diameters ranging from 1 to 10 μm with an average diameter about 3 μm.

## CONCLUDING REMARKS

The scaled-up terpolymerization of LA and bisphenol A derivatives resulted in moderate molecular weight TP. The resultant TP exhibited a higher $T_g$ versus PLA and a significantly higher thermal stability than PLA homopolymer. The modification of thermal properties and surface morphology did not alter the surface energy of the TP when compared with PLA despite the inclusion of fluorocarbon groups. Blending TP with PLA slightly enhanced the $T_g$ of the PLA matrix (ca. 5°C). Despite the moderate molecular weight, it was possible to successfully electrospin TP from chloroform and THF solutions to form microfiber nonwoven mats.

The authors thank Dr. Philip Brown and Mr. Saif Pathan for their help with electrospinning, Dr. Igor Luzinov for the access to AFM facility, and the Dow Chemical Co. and PolyMed., Inc., for the donation of starting materials.

## References

1. Mecking, S. Angew Chem Int Ed 2004, 43, 1078.
2. Carothers, W. H.; Dorough, G. L.; van Natta, F. J. J Am Chem Soc 1932, 54, 761.
3. Albertsson, A.-C.; Varma, I. K. Biomacromolecules 2003, 4, 1466.
4. Tsuji, H. In Biopolymers for Medical and Pharmaceutical Applications; Steinbüchel, A., Marchessault, R. H., Eds.; Wiley-VCH: Weinheim, 2005; Vol. 1, p 183.
5. Piorkowska, E.; Kulinski, Z.; Galeski, A.; Masirek, R. Polymer 2006, 47, 7178.
6. Abayasinghe, N. K.; Smith, D. W. Macromolecules 2003, 36, 9681.
7. O'Keefe, B. J.; Monnier, S. M.; Hillmyer, M. A.; Tolman, W. B. J Am Chem Soc 2001, 123, 339.
8. Tsuji, H.; Fukui, I. Polymer 2003, 44, 2891.
9. Park, P. I. P.; Jonnalagadda, S. J Appl Polym Sci 2006, 100, 1983.
10. Chen, B.-Q.; Kameyama, A.; Nishikubo, T. J Polym Sci Part A: Polym Chem 2000, 38, 988.
11. Nishikubo, T.; Kameyama, A.; Kawakami, S. Macromolecules 1998, 31, 4746.
12. Fish, R. H.; Dupon, J. W. J Org Chem 1988, 53, 5230.
13. Jedlinski, Z.; Kurcok, P.; Kowalczuk, M. Macromolecules 1985, 18, 2679.
14. Abayasinghe, N. K. PhD Dissertation, Clemson University, 2004.
15. Wilfong, R. E. J Polym Sci 1961, 54, 385.
16. Sperling, L. H. Introduction to Physical Polymer Science, 3rd ed.; Wiley-Interscience: New York, 2001.
17. Kaelble, D. H. Physical Chemistry of Adhesion; Wiley-Interscience: New York, 1971.
18. Owens, D. K.; Wendt, R. C. J Appl Polym Sci 1969, 13, 1741.
19. Li, W.-J.; Laurencin, C. T.; Caterson, E. J.; Tuan, R. S.; Ko, F. K. J Biomed Mater Res 2002, 60, 613.
20. Jaeger, R.; Schonherr, H.; Vancso, G. J. Macromolecules 1996, 29, 7634.